https://doi.org/10.1007/s11467-023-1276-4

RESEARCH ARTICLE

Anisotropic phonon thermal transport in two-dimensional layered materials

Yuxin Cai[1, *], Muhammad Faizan[1, *], Huimin Mu[2], Yilin Zhang[1], Hongshuai Zou[1], HongJian Zhao[2], Yuhao Fu[2, †], Lijun Zhang[1, ‡]

[1] State Key Laboratory of Integrated Optoelectronics, Key Laboratory of Automobile Materials of MOE, International Center of Computational Method and Software, School of Materials Science and Engineering, Jilin University, Changchun 130012, China

[2] State Key Laboratory of Superhard Materials, International Center of Computational Method and Software, College of Physics, Jilin University, Changchun 130012, China

Corresponding authors. E-mail: [†]fuyuhaoy@gmail.com, [‡]lijun_zhang@jlu.edu.cn

[*] These authors contributed equally.

Received January 24, 2023; accepted February 21, 2023

Special Topic:

Surface and Interface of Two-dimensional Materials (Eds.: Lijun Zhang, Dongchen Qi, Ming Yang & Kai Zhang).

Supporting Information

● Convergence tests of lattice thermal conductivity

To obtain strictly convergent κ_l, we carefully tested the effect of the truncation radius (R_{cutoff}) (used to calculate the third-order IFC and the q-point grid density of the Brillouin zone integral) on the calculated κ_l. We chose the truncation radius of 5 Å and the empirical value provided by previous studies [1-3], as shown in Fig. S1. The test results show that the κ_l is very sensitive to R_{cutoff}, and is highly overestimated at R_{cutoff} = 5 Å. The κ_l of the selected structures converges when the range of three-body interactions included in R_{cutoff} is large enough.

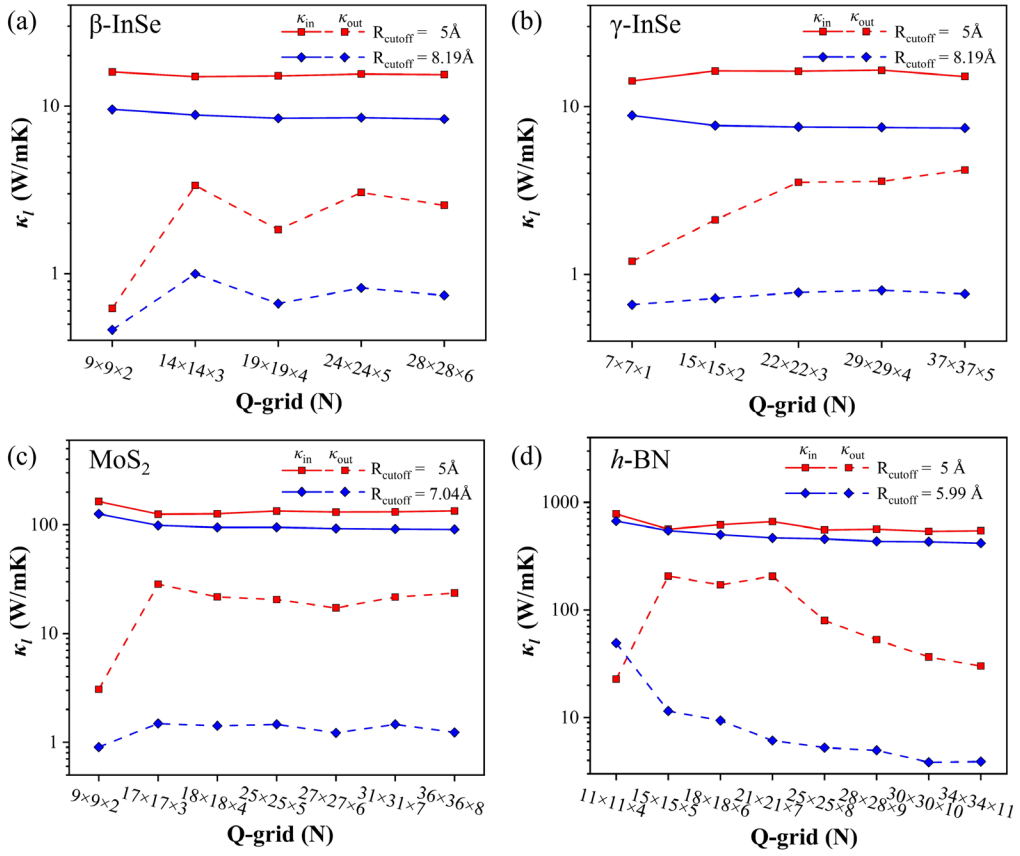

Fig. S1 Convergence test results of the thermal conductivity with respect to the q-mesh size and truncation radius (R_{cutoff}) for β-InSe, γ-InSe, MoS_2, and *h*-BN.

● Crystal structure and thermal transport coefficients of γ-InSe

In Fig. S2, we presented the crystal structure and thermal transport coefficients of γ-InSe. We found obvious anisotropy in the crystal structure, lattice thermal conductivity, phonon group velocity, and phonon lifetime of γ-InSe.

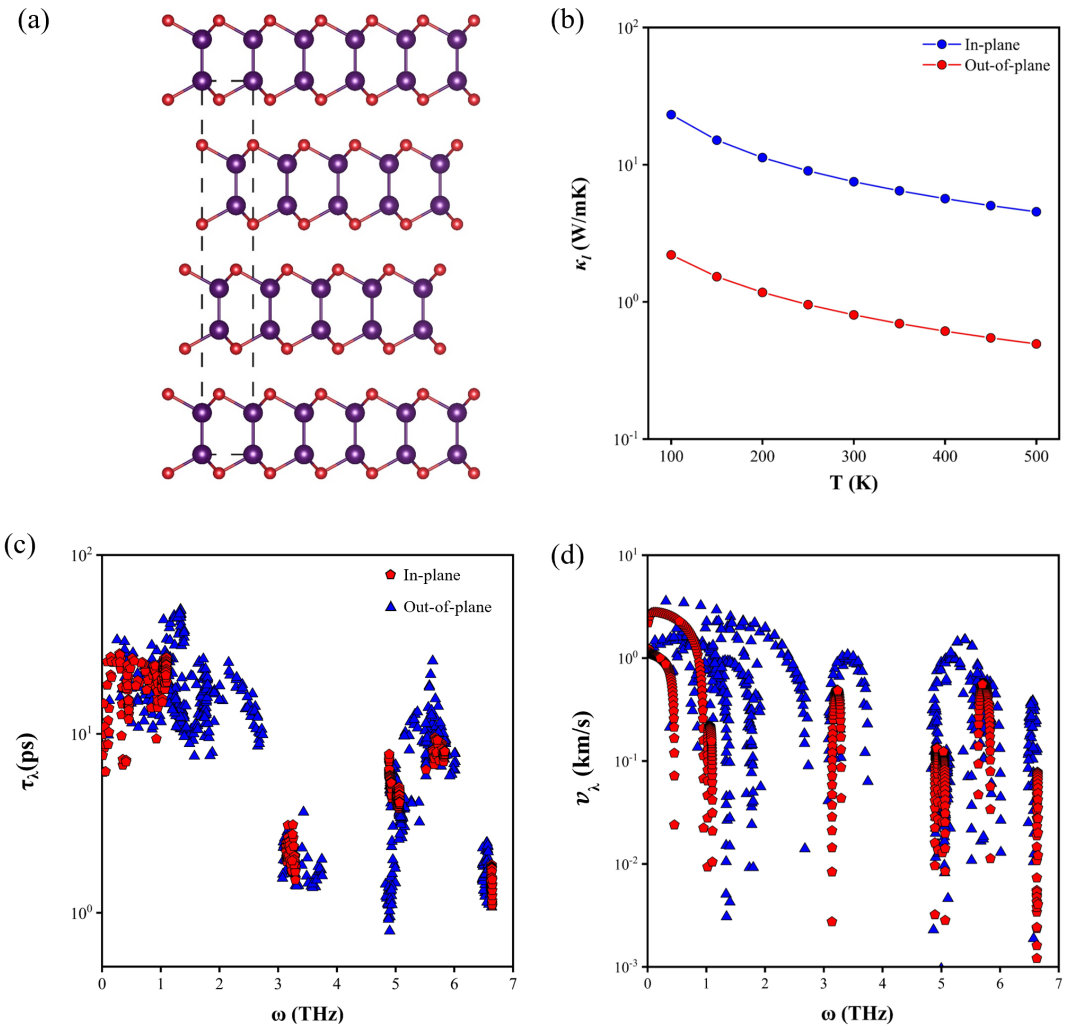

Fig. S2 (a) Crystal structure of the γ-InSe. (b) Lattice thermal conductivity of the γ-InSe as a function of temperature. (c) Phonon relaxation time and (d) group velocities of the γ-InSe as a function of frequency.

● Convergence tests of phonon dispersion

Our calculated phonon dispersion spectrum is plotted in Fig. S3. We note that for β-InSe and γ-InSe, imaginary frequencies appear near the point Γ point for a 3 × 3 × 1 supercell. Similarly, for *h*-BN, when a 4 × 4 × 2 supercell is used, imaginary frequencies appear near the Γ point. For MoS_2, no imaginary frequency is seen in the entire Brillouin zone.

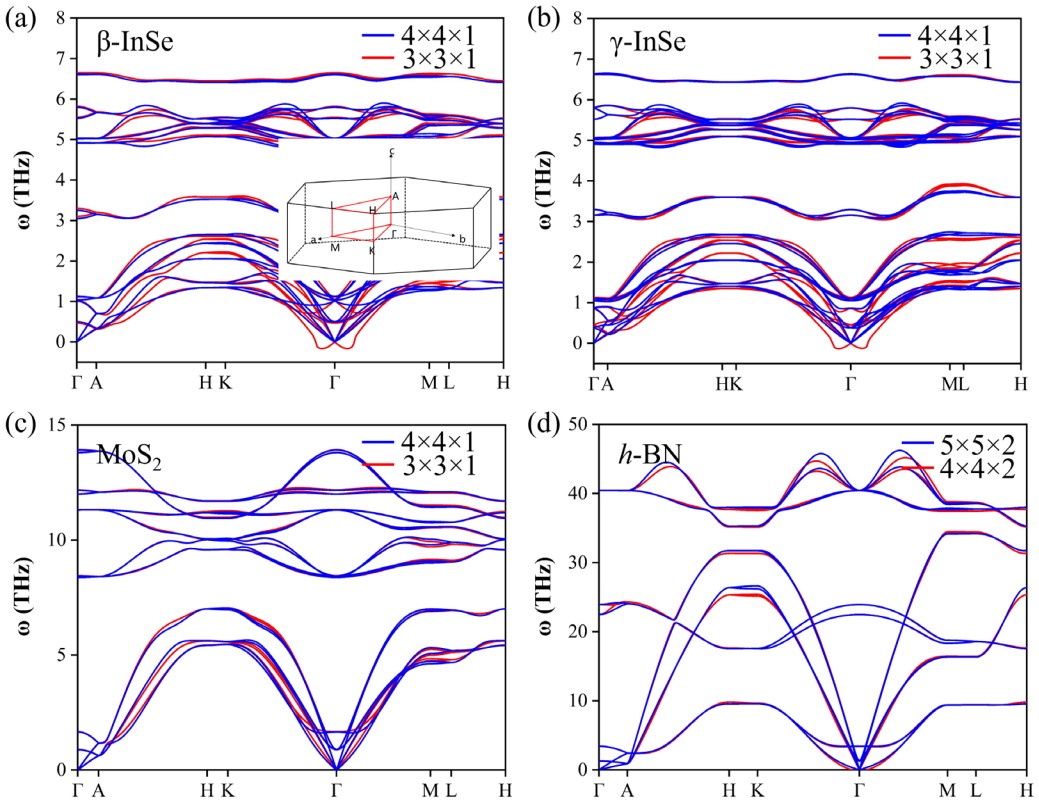

Fig. S3 Convergence tests of phonon dispersion spectrum with different supercell sizes for β-InSe, γ-InSe, MoS_2, and *h*-BN. High symmetry paths of the first Brillouin zone of β-InSe, γ-InSe, MoS_2, and *h*-BN unit cells are shown in the inset.

● Normalized cumulative κ_l as a function of frequency

It can be seen from Fig. S4 that the in-plane and out-of-plane cumulative κ_l of β-InSe, γ-InSe, MoS_2, and *h*-BN show obvious anisotropy with frequency. In addition, phonon transport in the low-frequency region dominates the κ_l of β-InSe, γ-InSe, MoS_2, and *h*-BN.

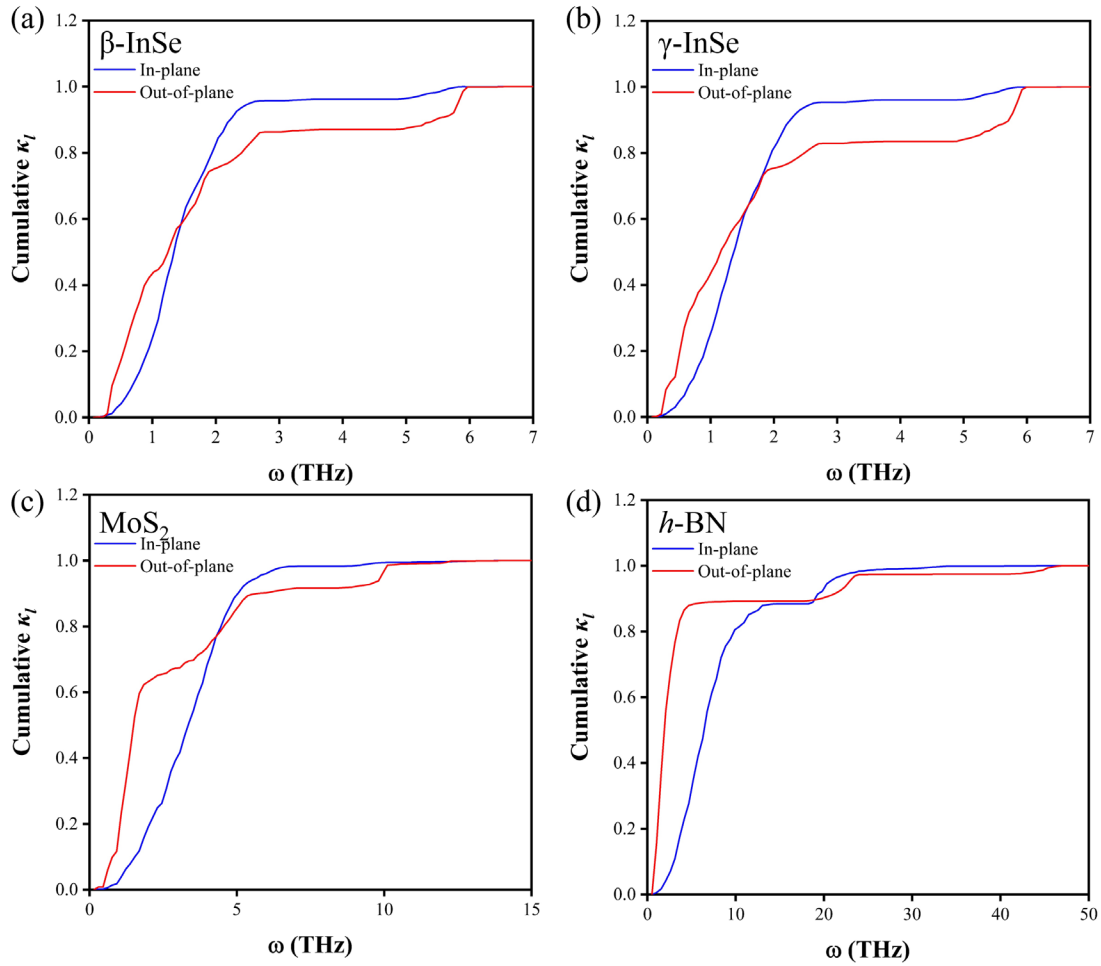

Fig. S4 Normalized cumulative lattice thermal conductivity with respect to the phonon frequency (ω) at 300 K for β-InSe, γ-InSe, MoS_2, and *h*-BN.

● Phonon group velocity as a function of frequency

From Fig. S5, it can be seen that the phonon group velocity in the in-plane direction of β-InSe, MoS_2, and *h*-BN is much larger than that in the out-of-plane direction. Therefore, the phonon group velocity is the dominant factor in anisotropic thermal transport.

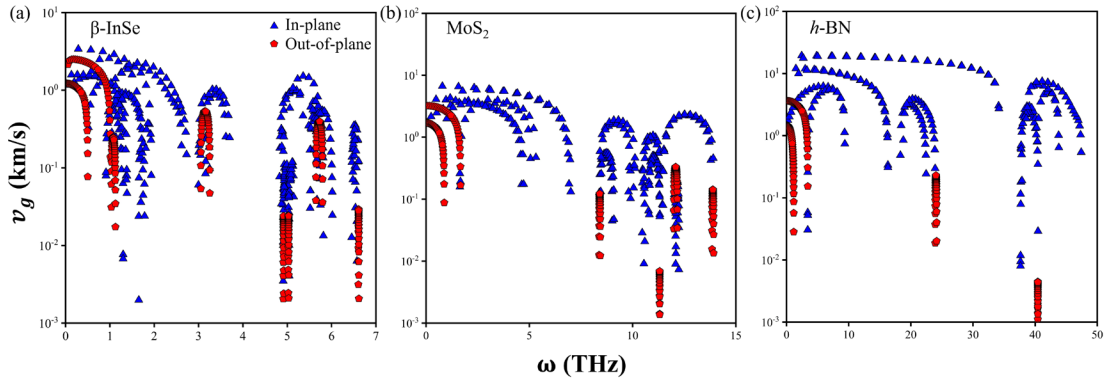

Fig. S5 The calculated group velocity of each phonon mode versus phonon frequency (ω) for β-InSe, MoS_2, and *h*-BN.

● Size effect of lattice thermal conductivity

Based on the phonon mean free path uniparametric equation [4], we evaluated the normalized anisotropic lattice thermal conductivity as a function of thickness for β-InSe, γ-InSe, MoS_2, and *h*-BN, and plotted the data in Fig. S6.

$$\kappa_l(L) = \frac{\kappa_l^{max}}{1+\frac{rMFP}{L}}, \tag{S1}$$

where κ_l is the cumulative lattice thermal conductivity, κ_l^{max} is the maximum lattice thermal conductivity (corresponding bulk system). And rMFP is a representative mean phonon-free path, as shown in Table S5. The results show that the thickness-dependent lattice thermal conductivities of β-InSe, γ-InSe, MoS_2, and *h*-BN still have anisotropy in both the in-plane and out-of-plane directions. As the sample thickness decreases, the phonon boundary scattering increases, and the lattice thermal conductivity decreases. For instance, when the sample size is 60, 120, and 200 nm, the lattice thermal conductivities in the out-of-plane direction of β-InSe are 0.54, 0.63, and 0.79 W/mK, respectively. It is close to the experimental value reported by Rai et al. [5], proving the reliability of our theoretical results. When the sample size is about 10^6 nm, the lattice thermal conductivity of the four structures converges to the value of the bulk system.

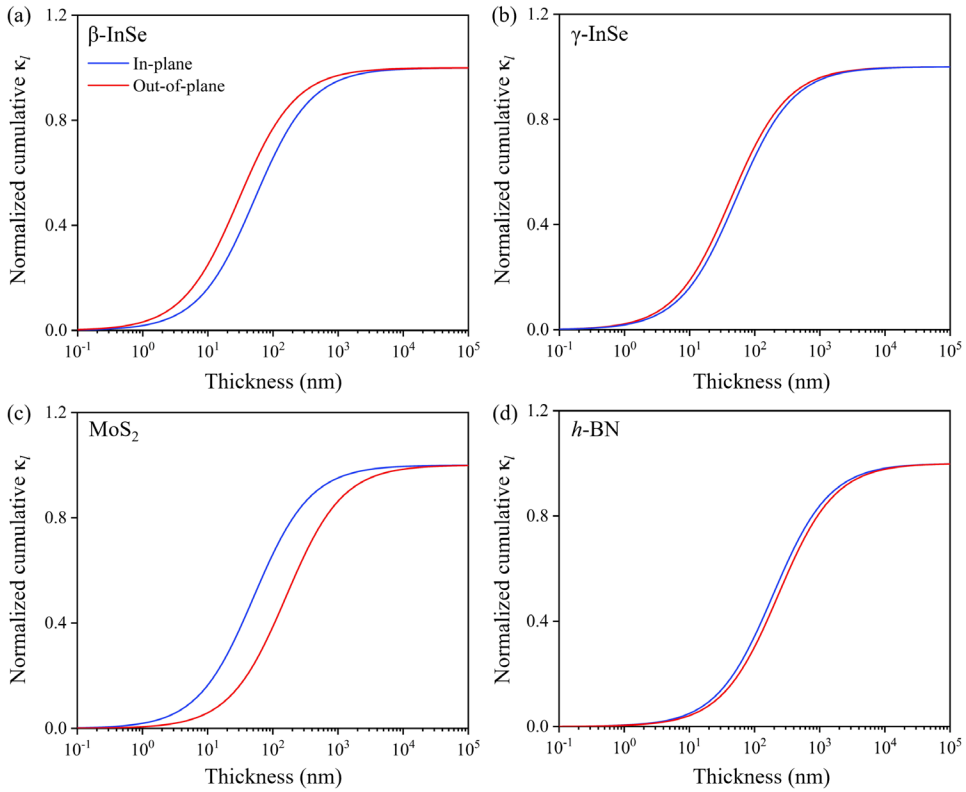

Fig. S6 Normalized cumulative lattice thermal conductivity of bulk (a) β-InSe, (b) γ-InSe, (c) MoS_2, and (d) *h*-BN as a function of thickness at 300 K.

Table S1 The calculated lattice parameters of β-InSe, γ-InSe, MoS_2, and *h*-BN optimized using optB86b-vdW and optB88-vdW functionals along with experimental results. Our calculated lattice parameters from optB86b-vdW functional are more consistent with the experimental values than optB88-vdW.

Structure	Method	a (Å)	b (Å)	c (Å)
β-InSe	OptB86b-vdw	4.04136	4.04136	16.90498
	OptB88-vdw	4.07134	4.07134	16.96122
	Exp. [6]	4.04	4.04	16.93
γ-InSe	OptB86b-vdw	4.04658	4.04658	25.12748
	OptB88-vdw	4.07615	4.07615	25.22617
	Exp. [7]	4.002	4.002	24.961
h-BN	OptB86b-vdw	2.51268	2.51268	6.45828
	OptB88-vdw	2.51207	2.51207	6.55024
	Exp. [8]	2.504	2.504	6.661
MoS_2	OptB86b-vdw	3.16447	3.16447	12.37900
	OptB88-vdw	3.19095	3.19095	12.47176
	Exp. [9]	3.15	3.15	12.3

Table S2 The Born effective charge *Z** (in the unit of elementary charge e) and dielectric constant ε of bulk β-InSe, γ-InSe, MoS_2, and *h*-BN. The longitudinal and transverse optical splitting is predicted by incorporating the effects of long-range Coulomb interactions based on the ε and *Z** calculated by the first-principles method.

Structure	Atom	$Z^*_{xx} = Z^*_{yy}$	Z^*_{zz}	$\varepsilon_{xx} = \varepsilon_{yy}$	ε_{zz}
β-InSe	In	-2.39	-1.22	8.21	17.54
	Se	2.39	1.22		
γ-InSe	In	-2.39	-1.37	8.4	19.82
	Se	2.41	1.19		
MoS_2	Mo	0.99	0.61	15.14	6.39
	S	-0.49	-0.30		
h-BN	B	2.71	0.72	4.71	2.63
	N	-2.71	-0.72		

Table S3 The comparison between theoretical and experimental values of κ_{in} and κ_{out} (W/mK) for β-InSe, MoS_2, and *h*-BN at 300K. For β-InSe, MoS_2, and *h*-BN, our calculated κ_l at 300K exhibit highly anisotropic properties, which are in good agreement with previous experimental reports, demonstrating the reliability of our DFT approach.

Structure	Method	κ_{in}	κ_{out}
β-InSe	Cal.	8.6	0.8
	Exp. [5]	8.5±2	0.76±0.15
MoS_2	Cal.	94.8	1.2
	Exp. [10]	110±20	2±0.3
h-BN	Cal.	428.2	3.9
	Exp. [11]	420±46	4.8±0.6

Table S4 The elastic constant C_{in} (Gpa) in the in-plane direction and mass per unit area $\bar{m}$(10^{-6} kg·m^{-2}) of β-InSe, MoS_2, and *h*-BN. The elastic constant of the structure helps to explain the numerical gap of the phonon group velocity in the in-plane direction. We found that the numerical value of the elastic constant conforms to $C_{\mathrm{InSe}} < C_{\mathrm{MoS_2}} < C_{h-\mathrm{BN}}$. The calculated $\bar{m}$ show opposite trend with the elastic constants, and a heavy $\bar{m}$ will lead to a low phonon frequency and small lattice thermal conductivity.

Structure	C_{in}	$\bar{m}$
β-InSe	62	4.5
MoS_2	224	3.1
h-BN	859	0.8

Table S5 Representative mean free path (rMFP) of the β-InSe, γ-InSe, MoS_2, and *h*-BN. We define the phonon-free path corresponding to 50% of the total thermal conductivity as rMFP.

rMFP (nm)	In-plane	Out-of-plane
β-InSe	52	30
γ-InSe	43	22
MoS_2	51	159
h-BN	192	231

● Average Phonon Group Velocity and Phonon Lifetime

The average phonon group velocity ($\bar{\boldsymbol{v}}_{\boldsymbol{\lambda}}$) and phonon lifetime ($\bar{\boldsymbol{\tau}}_{\boldsymbol{\lambda}}$) are given by [12,13]

$$\bar{\boldsymbol{v}}_{\boldsymbol{\lambda}} = \sqrt{\frac{\sum_{\lambda} \boldsymbol{C}_{\lambda} \boldsymbol{v}_{\lambda}^{2}}{\sum_{\lambda} \boldsymbol{C}_{\lambda}}}, \tag{S2}$$

and

$$\bar{\boldsymbol{\tau}}_{\boldsymbol{\lambda}} = \frac{\sum_{\lambda} \boldsymbol{C}_{\lambda} \boldsymbol{\tau}_{\lambda}}{\sum_{\lambda} \boldsymbol{C}_{\lambda}}. \tag{S3}$$

$\boldsymbol{\lambda}$: is a phonon mode, $\boldsymbol{C}_{\boldsymbol{\lambda}}$: phonon mode-specific heat capacity, $\boldsymbol{v}_{\boldsymbol{\lambda}}$: represents the phonon group velocity, $\boldsymbol{\tau}_{\boldsymbol{\lambda}}$: the phonon relaxation time.

References

1. S. Chen, A. Sood, E. Pop, K. E. Goodson, and D. Donadio, Strongly Tunable Anisotropic Thermal Transport in MoS_2 by Strain and Lithium Intercalation: First-Principles Calculations, *2D Mater*. 6(2), 025033 (2019)
2. B. Niu, L. Zhong, W. Hao, Z. Yang, X. Duan, D. Cai, P. He, D. Jia, S. Li, and Y. Zhou, First-Principles Study of the Anisotropic Thermal Expansion and Thermal Transport Properties in h-BN, *Sci. China Mater.* 64(4), 953 (2021)
3. W. Wan, S. Zhao, Y. Ge, and Y. Liu, Phonon and Electron Transport in Janus Monolayers Based on InSe, *J. Phys.: Condens. Matter* 31(43), 435501 (2019)
4. W. Li, J. Carrete, N. A. Katcho, and N. Mingo, ShengBTE: A Solver of the Boltzmann Transport Equation for Phonons, *Comput. Phys*. 185(6), 1747 (2014)
5. A. Rai, V. K. Sangwan, J. T. Gish, M. C. Hersam, and D. G. Cahill, Anisotropic Thermal Conductivity of Layered Indium Selenide, Appl. Phys. Lett. 118(7), 073101 (2021)
6. S. A. Semiletov, Determination of the structure of InSe by electron diffraction, *Sov. Phys. Crystallogr. Krist.* 3, 292 (1958)
7. G. W. Mudd, S. A. Svatek, T. Ren, A. Patane, O. Makarovsky, L. Eaves, P. H. Beton, Z. D. Kovalyuk, G. V. Lashkarev, Z. R. Kudrynskyi and A. I. Dmitriev, Tuning the Bandgap of Exfoliated InSe Nanosheets by Quantum Confinement, *Adv. Mater.* 25(40), 5714 (2013)
8. R, S, Pease. An X-ray study of boron nitride, *Acta Crystallographica*. 5, 356 (1952).
9. K. D. Bronsema, J. L. De Boer, and F. Jellinek, On the Structure of Molybdenum Diselenide and Disulfide, *Z. Anorg. Allg. Chem.* 540(9-10), 15 (1986)
10. J. Liu, G. Choi, and D. G. Cahill, Measurement of the Anisotropic Thermal Conductivity of Molybdenum Disulfide by the Time-Resolved Magneto-Optic Kerr Effect, *J. Appl. Phys.* 116(23), 233107 (2014)
11. P. Jiang, X. Qian, R. Yang, and L. Lindsay, Anisotropic Thermal Transport in Bulk Hexagonal Boron Nitride, *Phys. Rev. Materials* 2(6), 064005 (2018)
12. A. G. Gokhale, D. Visaria, and A. Jain, Cross-Plane Thermal Transport in MoS_2, *Phys. Rev. B* 104(11), 115403 (2021)
13. R. Guo, X. Wang, Y. Kuang, and B. Huang, First-Principles Study of Anisotropic Thermoelectric Transport Properties of IV-VI Semiconductor Compounds SnSe and SnS, *Phys. Rev. B* 92(11), 115202 (2015)